Journal of Statistical Physics, Vol. 64, Nos. 5/6, 1991

Novel States in Taylor–Couette Flow Subjected to a Coriolis Force

Li Ning,[1] Guenter Ahlers,[1] and David S. Cannell[1]

We present experimental results for Taylor–Couette flow subjected to a Coriolis force. We used an apparatus consisting of two concentric cylinders with the inner one rotating, and with a radius ratio near 0.75. It was mounted with its axis horizontal on a table which rotated with angular velocity Ω about a vertical axis. For sufficiently low Ω, the first bifurcation upon increasing the inner-cylinder rotation rate ω was to tilted vortices. With further increase in ω this bifurcation was followed by a secondary one to time-periodic tilted vortices. The two bifurcation lines met at higher Ω. The initial bifurcation then became one to tilted traveling vortices. For even larger values of Ω, the flow immediately above the initial transition was disordered, and for sufficiently large Ω the initial bifurcation was to a featureless turbulent state. We studied these transitions with three different outer cylinders. Two had symmetric spatial ramps terminating both ends of a straight section to reduce the effect of the rigid, non-rotating ends, and one had no ramps. The transition to featureless turbulence in the apparatus with ramps became hysteretic over a range of Ω.

KEY WORDS: Taylor–Couette flow; Coriolis force; Taylor vortices; tilted vortices; chaotic vortices; traveling vortices; spatially ramped control parameter; featureless turbulence.

1. INTRODUCTION

In the study of hydrodynamic stability in the presence of external fields, Coriolis and magnetic effects are of particular interest because they occur frequently in nature, and because they can profoundly influence flows. In this paper we report on a study of the effect of a Coriolis force, which is present when the fluid system is in a rotating frame. The rotation often inhibits the instability and alters the nonlinear state beyond the bifurcation.

[1] Department of Physics and Center for Nonlinear Science, University of California, Santa Barbara, California 93106.

0022-4715/91/0900-0927$06.50/0

Rayleigh–Bénard convection[1,2],[2] (RBC) in a fluid heated from below and rotated about a vertical axis is a system which has received significant theoretical[4–6] and experimental[7–10] attention in this field. Here we report upon the effect of external rotation upon Taylor-vortex flow[11],[3] (TVF). This flow occurs as the result of an instability of circular Couette flow,[14] i.e., in a fluid contained between two concentric cylinders with one or both of them rotating. When these cylinders are placed in a rotating frame, with the additional rotation axis orthogonal to the cylinder axes, a Coriolis force acts upon the fluid due to the coupling between the external rotation and the azimuthal flow in the Couette state. It was suggested to one of us by P. Marcus[4] that this system should have interesting properties because the Coriolis force breaks the cylindrical symmetry which prevails for TVF in a stationary frame.

The TVF system in a rotating frame was investigated recently in experiments by Wiener *et al.*[15,16] Their work aimed primarily at exploring the similarities to RBC in the presence of rotation, and at determining the details of the stability behavior in narrow-gap geometries (radius ratio of 0.883 and 0.950). It was reported[15] that the stabilizing effect of the rotation on the first instability had a similar dependence upon the external rotation rate Ω as the theoretical[4] and experimental[9] results for rotating RBC, and that above a certain value of Ω the base flow lost its stability, via a direct transition to turbulence without any precursor instabilities when the inner-cylinder rotation rate ω was increased.[16] The experiment was carried out in an apparatus with an axially uniform gap between the two concentric cylinders, and it was observed that the transition to turbulence was triggered by the irregular flows generated at the fixed end boundaries.[17]

From a theoretical viewpoint, TVF with a Coriolis force has been examined only very recently. Brand[18],[5] and Wiener *et al.*[16] independently calculated corrections to the circular Couette state to first order in Ω. Wiener *et al.* are continuing this work to higher order.[19],[6] Ning *et al.*[20,21] calculated this base flow to order Ω^2, and also determined its stability to

[2] A large literature pertaining to this field has evolved. Particularly useful as introductions to early work are the reviews in refs. 3.

[3] A sizable literature now exists dealing with this system. A comprehensive review has been given by DiPrima and Swinney.[12] Important early papers in this field are numerous; but particularly noteworthy are refs. 13.

[4] P. S. Marcus, private communication to G.A., January 30, 1987.

[5] This work was presented at the First Symposium on Görtler-Vortex Flows, cochaired by H. Peerhossaini and J. E. Wesfreid, Euromech 261 and NATO ARW, June 11–14, 1990, Nantes, France.

[6] These authors also plan to carry out a stability analysis.

order Ω^2. The theoretical results of Ning *et al.* are compared with the experimental measurements in another publication.[21] In the present paper we present our experimental work in somewhat greater detail, and make only a very brief comparison with the theory.

In part, the purpose of our experiment was to answer the question of whether the reported direct transition to turbulence was a bulk property or a boundary effect. If the former were true, then we would have a system which had turbulent states evolving directly from a relatively simple base state, perhaps suitable for a quantitative study of the turbulent onset under conditions of weak nonlinearity. To achieve this purpose, we employed Couette systems with two identical spatially-ramped outer-cylinder sections attached one to each end of a straight central outer-cylinder section. The ramps provided "soft" boundary conditions by smoothly decreasing the Reynolds number as a function of axial position below its critical value.[22–24] This nearly eliminated phase pinning and the influence of the Ekman vortices which exist at the ends. It also permitted the tilted vortices which form above the first bifurcation at modest rotation rates to assume their natural tilt angle, unimpeded by the vertical collars at the ends. The other purpose of our investigation was to extend the available quantitative information about the bifurcation lines and the system properties to a smaller radius ratio than those of Wiener *et al.*[15,16] Here we were particularly interested in modest rotation rates where a comparison with parallel theoretical work[20] seems feasible.

2. APPARATUS AND EXPERIMENTAL METHOD

In our investigations, two concentric cylinders were placed, with their axes horizontal, on a table rotating about a vertical axis. The outer cylinder was always stationary except for the overall table rotation. The inner one rotated about its axis. The inner cylinder had a constant radius independent of axial position and was the same for all of our experiments. We used three different outer cylinders, to which we will refer as apparatus I, II, and III. Apparatus I had an outer cylinder of uniform radius. The outer cylinder of apparatus II had ends consisting of inwardly tapered sections in which the inner diameter decreased linearly away from the end of the straight section with a ramp angle of 0.014 rad. In apparatus III we used double-parabolic ramps with the profiles shown schematically in Fig. 1. The larger-diameter ends of the ramped sections were glued to the straight center section. In all cases, the outer ends of the ramped sections of the apparatus were terminated by rigid, nonrotating collars, which essentially filled the gap. The radius ratios of the cylinders were close to 0.75 in the straight section. The geometric parameters of the three apparatus are sum-

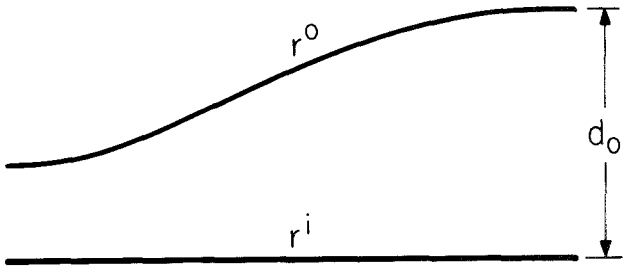

Fig. 1. Schematic diagram of the double-parabolic ramps of apparatus III.

marized in Table I, where r is the radius, d is the gap between the two cylinders, l is the length of the section, superscripts i and o stand for inner and outer cylinder, respectively, and subscripts 0 and t denote parameters in the straight and tapered sections, respectively.

The two control parameters in this experiment are the Reynolds number associated with the inner-cylinder rotation and the dimensionless angular frequency Ω of the table rotation.[7] They are defined as $R \equiv r_0^i \tilde{\omega} t_g / d_0$ and $\Omega \equiv \tilde{\Omega} t_g$, respectively. Here $\tilde{\omega}$ and $\tilde{\Omega}$ are the angular speeds, in rad/sec, of the inner cylinder and the table, respectively, $t_g = d_0^2/\nu$, $d_0 = r_0^o - r_0^i$, and ν is the kinematic viscosity of the fluid.

The working temperature was near 22°C, and the fluid was 98% water seeded with 2% by volume Kalliroscope suspension[8] (see also ref. 25) to visualize the flow. Taking into consideration the effect[26] of the Kalliroscope on ν, the viscosity was 0.0092 cm^2/sec. Thus, t_g was 43, 41, and 49 sec for apparatus I, II, and III, respectively. The temperature of the fluid was measured with a resolution of better than 0.001 K using thermistors imbedded in stainless steel tubes and immersed in the fluid at both

[7] In refs. 15 and 16 a Taylor number was defined as equal to $4\Omega^2$. A different Taylor number is often used to describe the *inner-cylinder* rotation rate (for which we are using R in the present paper). In order to avoid confusion, we prefer not to use an additional Taylor number for the *table* rotation rate.

[8] Kalliroscope Corporation, P.O. Box 60, Groton, Massachusetts, rheoscopic liquid AQ-1000.

Table I. Dimensions of the Apparatus

Apparatus	r_0^i (cm)	d_0 (cm)	r_0^i/r_0^o	l_0 (cm)	l_t (cm)	Outer cylinder shape
I	1.869	0.631	0.746	33.82	—	Straight
II	1.869	0.616	0.753	12.60	14.0	Linear ramps
III	1.869	0.673	0.736	16.43	13.4	Parabolic ramps

ends outside the fixed collars. The measured temperature difference across the apparatus was no larger than 0.2 K at any time, and was reduced to typically less than 50 mK during the later stages of the investigation. Due to the difficulty of having a fixed-temperature bath on a rotating table, we chose to operate at the normal room temperature (which varied typically by less than 1 K) and to regulate $\tilde{\Omega}$ and $\tilde{\omega}$ so as to keep Ω and R constant. The temperatures were measured every 5 sec, the kinematic viscosity of the fluid was calculated using the averaged temperature, and the speeds of the driving motors were adjusted accordingly. Some measurements on spatial patterns were made on certain states prepared with the regulation. The same measurements were later performed on the same states after the regulation was turned off. There was much less scatter in the data acquired with regulation.

The flow pattern was imaged by a video camera (Panasonic, model WV1460) mounted on the rotating table. The image was captured and digitized by a video-capture system (Chorus Data Systems, Inc., PC-EYE) housed in the controlling computer. For the determination of bifurcation points at constant Ω, we initially chose a step size for $\tilde{\omega}$ of 0.5% of the estimated critical rotation rate and slowly ramped the inner-cylinder rotation rate from one step to the next with a typical ramp rate of $(1/\tilde{\omega})$ $d\tilde{\omega}/dt < 0.02$ (t is in units of t_g). After waiting for a stationary state at each step (typically $10t_g$), one or more images were acquired. From each image, a one-dimensional array, or contour line, representing the intensity of the light reflected by the Kalliroscope as a function of axial position, was extracted by averaging a few adjacent image lines. In such a contour line for a TVF state, the dark portions represent radial inflow and outflow regions. The Fourier transform F of the contour line was computed. Near the wavenumber q of the pattern, $|F|$ grew sharply at the first appearance of the vortex structure, and the area S_q under the peak of $|F|$ corresponding to q could be determined. Once S_q grew over a certain empirical threshold, we reduced the step size and quasistatically ramped down in smaller steps, measuring S_q as before. We chose the onset of the instability of the structureless base flow as the point where a straight line fitted to $S_q(\tilde{\omega})$ intersected a baseline value S_0 determined below the bifurcation point by summing $|F|$ over the same interval of wavenumbers used to determine S_q. An example of experimental values of $S_q(\tilde{\omega})$ is given in Fig. 2. An analogous method could be applied at constant $\tilde{\omega}$ by determining $S_q(\tilde{\Omega})$.

The spectral method described above also gave the wavenumber associated with the spatially periodic pattern. A similar technique was used to analyze time series of the signal measured at one spatial point, and gave the onset of time-dependent states and the corresponding frequencies. The

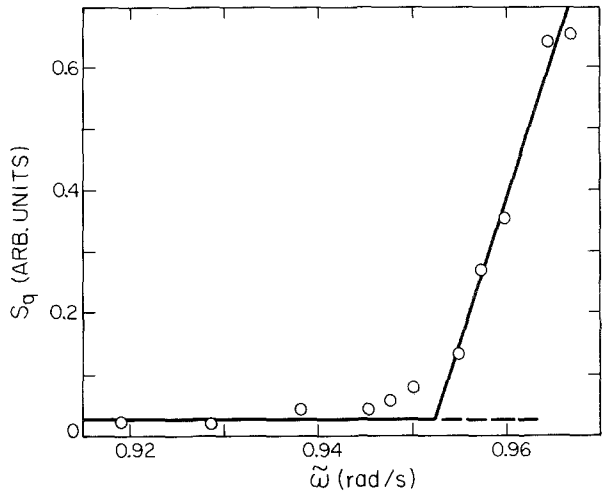

Fig. 2. The area S_q under the peak of the absolute value of the Fourier transform F corresponding to the wavenumber q of the first instability, as a function of the inner-cylinder rotation rate $\tilde{\omega}$. These data are for $\Omega \cong 5$. The horizontal line is the threshold discussed in the text, and the other solid line is a fit to the five largest values.

time dependence of the phase associated with the spatial period of the pattern was used to determine the velocity of traveling waves. In addition to the Fourier-transform techniques, examination of contour plots (a temporal sequence of contour lines plotted horizontally with a vertical displacement of successive ones) was often useful for the determination and display of the pattern.

By placing the center of apparatus II at a position on the table which was on the one hand a distance of about 25 cm from the table center, and on the other coincident with the table center, we confirmed experimentally the expectation that the centrifugal acceleration does not influence the system significantly. In the two cases, the bifurcations from a structureless base flow to a spatially nonuniform secondary flow agreed with each other within our experimental uncertainty ($\pm 0.25\%$) for a range of Ω from 0 to 50. There also was no visual difference in the flow patterns which formed above the bifurcation. Most of our measurements were made with the on-center position of the apparatus.

3. RESULTS

In the remainder of this paper we describe our findings in the order of increasing R and Ω. Our results are from the apparatus with linear ramps (apparatus II) unless otherwise mentioned. When a transition is described,

the changing parameter (R or Ω) will be given, while the other one is implied to be fixed. It is worth pointing out that, since the critical wavenumber of the secondary flow varies with the table rotation rate, and since some of the secondary bifurcations are hysteretic, one can sometimes make different states at the same point in the parameter space by following different paths. In our experiment, the states were usually prepared by quasistatically ramping R up from below its critical value while keeping Ω fixed. Experimental results for the overall bifurcation diagram are given in Fig. 3. Figures 4 and 5 are enlargements of Fig. 3 showing special features.

3.1. Small Ω

At small Ω ($\lesssim 8.5$), the first transition upon increasing R was a bifurcation from the structureless base flow to tilted Taylor vortices (STV or DTV in Fig. 3). The tilt direction reversed when the direction of either the

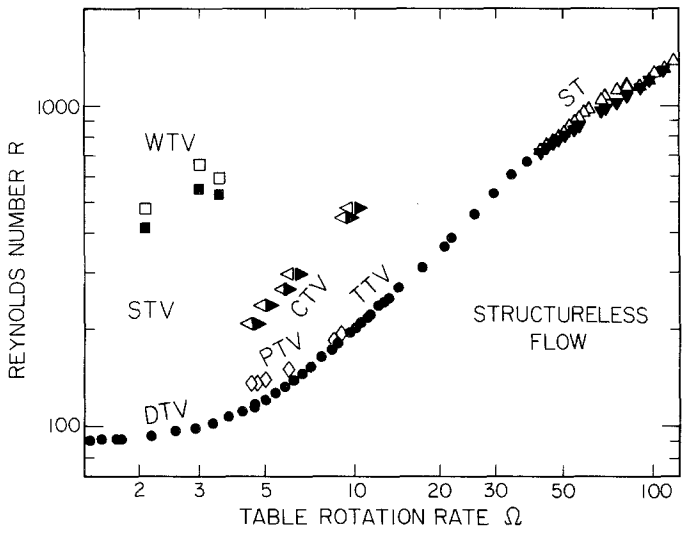

Fig. 3. Experimental results for the bifurcation lines in the Reynolds number–Ω plane. This figure covers the entire range of our experiments; details are given in Figs. 4 and 5. The data are from apparatus II. The solid circles are a nonhysteretic primary bifurcation which leads to very slowly drifting tilted vortices (DTV) at small Ω, and to time-periodic tilted vortices (PTV) or traveling tilted vortices (TTV) of much higher frequency for $\Omega \gtrsim 8.5$. The triangles for $\Omega \gtrsim 40$ are a hysteretic primary bifurcation to structureless turbulence (ST) (open: R increasing; closed: R decreasing). The squares are a hysteretic secondary bifurcation to wavy tilted vortices (WTV) (open: R increasing; solid: R decreasing). The triangles for $4 \lesssim \Omega \lesssim 10$ are a hysteretic secondary bifurcation between a chaotic tilted vortex state (CTV) and a steady tilted vortex state (STV). The diamonds are a secondary nonhysteretic bifurcation to time-periodic tilted vortices (PTV) which meets the primary bifurcation near $\Omega = 8.5$.

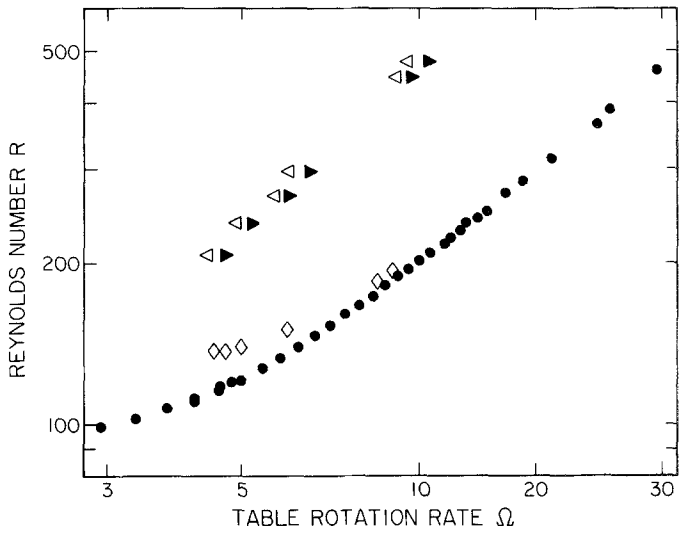

Fig. 4. Details of the bifurcation lines for intermediate values of Ω. The data are from apparatus II. The symbols are as in Fig. 3.

inner-cylinder rotation or the table rotation was reversed, but remained the same when both rotation directions were changed. In this range of Ω, the critical Reynolds number R_c is nearly a quadratic function of Ω. This is consistent with the expectation that R_c is invariant under the transformation $\Omega \rightarrow -\Omega$. It is shown explicitly in Fig. 6, which gives R_c vs. Ω^2. Those

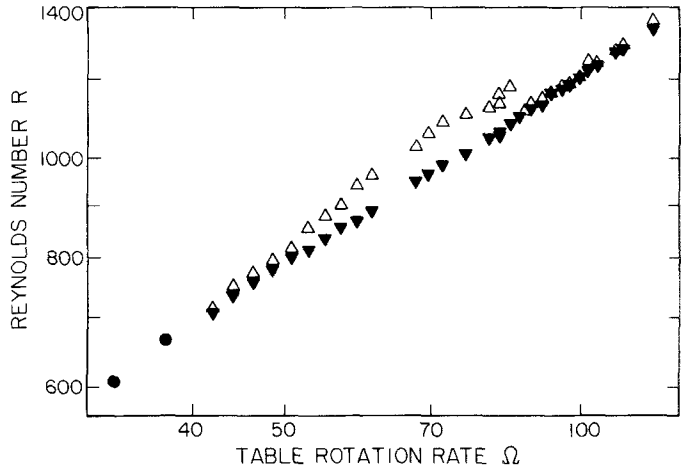

Fig. 5. Details of the bifurcation lines at large Ω where there is a direct transition from the base state to a structureless turbulent state. The data are from apparatus II. The symbols are as in Fig. 3.

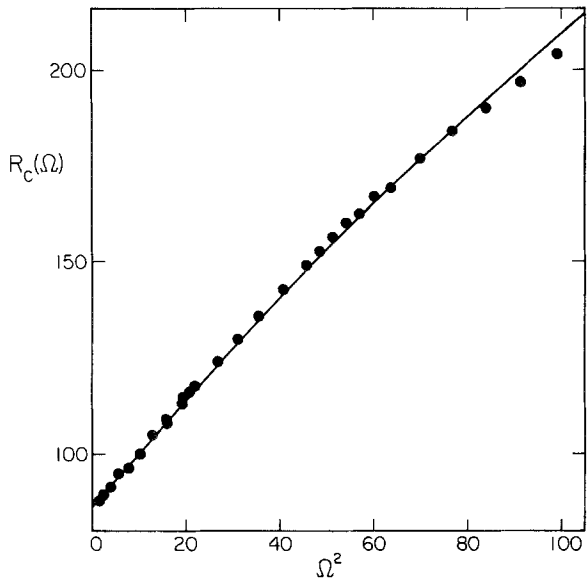

Fig. 6. The critical Reynolds number R_c as a function of Ω^2. The line through the data is a fit of Eq. (1) to the measurements with $\Omega^2 < 25$. The data are from apparatus II.

data are for apparatus II positioned with its center on the rotation axis. The results for $0.7 < \Omega < 5$ were fit to the function

$$R_c = R_{c0}\{1 + (\Omega/\Omega_0)^2\,[1 + c(\Omega/\Omega_0)^2]\} \tag{1}$$

The line in the figure is the result of this fit. It gave $R_{c0} = 86.21$, $\Omega_0 = 7.75$, and $c \cong -0.08$. When equivalent results for $R_c(\Omega)$ for apparatus II in the *off*-center position on the rotation table were analyzed similarly, they yielded $R_{c0} = 86.77$, $\Omega_0 = 7.60$, and $c \cong -0.07$. The agreement between the two sets of data provides further quantitative evidence for the fact that the centrifugal acceleration is unimportant in this instability. The theoretical result[27] $R_{c0} = 86.33$ for $\eta = 0.753$ is in excellent agreement with our measurements. When the theoretical values[20] of $R_c(\Omega)$ for $\Omega < 5$ were fit to Eq. (1), they yielded $\Omega_0 = 7.75$ for $\eta = 0.753$, also in excellent agreement with the experiment.

In Fig. 7, which gives Ω_0 vs. η, we plot our result for Ω_0 as a solid circle, and those of Wiener *et al.*[15] as open circles. The line in the figure is the theoretical result.[20] The values of Wiener *et al.* are slightly below the theory. A reason for this may be that these authors, although they fitted an equation similar to Eq. (1) to their data, omitted the term of fourth order in Ω. Such a fit would give an effective value of Ω_0 slightly below the value

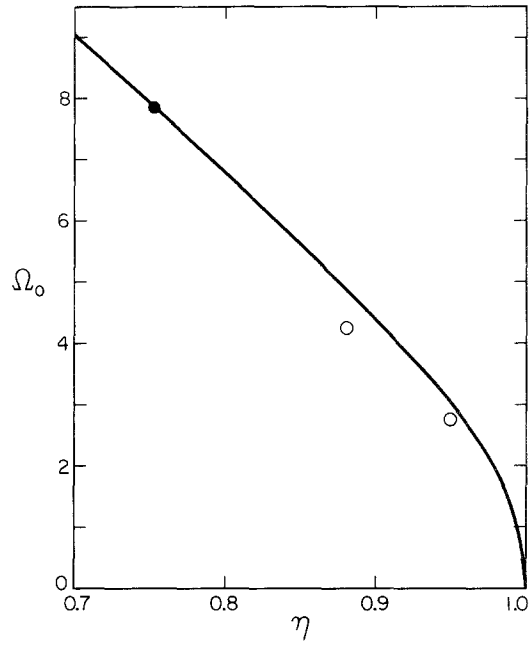

Fig. 7. The parameter Ω_0 in Eq. (1) as a function of the radius ratio η. The data at $\eta = 0.95$ and 0.88 are from ref. 15. The solid line is from ref. 20.

relevant in the limit as Ω vanishes, because $c > 0$ for their radius ratios. Thus we believe that all experimental data agree with the theory within their allowed systematic and random errors.

Without rotation, TVF and RBC are most nearly comparable in the narrow-gap limit.[9] For TVF with rotation, Ω_0 vanishes in that case.[20] On the other hand, for RBC one has[4] $\Omega_0 \cong 30$. Thus, we see that the two systems differ dramatically in their response to a Coriolis force. An important physical difference between the two systems is that in RBC the Coriolis force has no influence on the state below the primary bifurcation (conduction state), whereas in TVF the Coriolis force couples to the circular Couette flow and thus makes the base flow dependent upon Ω.

We have also measured the critical wavenumber $q_c(\Omega)$ at small Ω, and those results are shown in Fig. 8. We see that q_c decreases significantly with Ω. In the RBC case, the opposite dependence is found, i.e., q_c increases[4] with Ω. The experiment suggests that the initial decrease of q_c with Ω is

[9] The two systems are strictly equivalent (in the absence of rotation) in the narrow-gap limit and for the case where the inner and outer cylinders are rotated with the same angular speed.

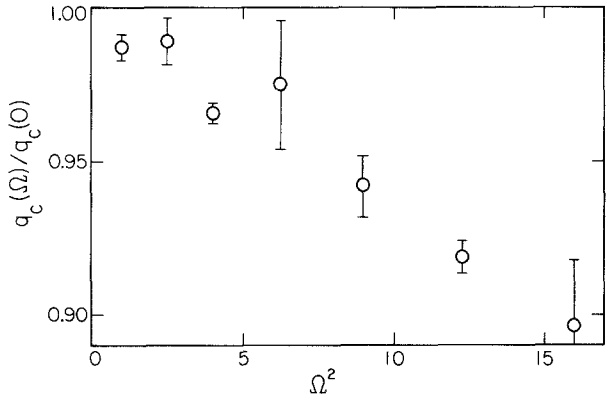

Fig. 8. The critical wavenumber of the vortices in the axial direction as a function of Ω^2. The data are from apparatus II.

quadratic in Ω. This is consistent with the expectation that q_c as well as R_c is invariant under the transformation $\Omega \to -\Omega$.

An interesting feature of the nonlinear state immediately above the bifurcation and for $\Omega \gtrsim 3$ is that the tilted vortices in apparatus II and III drift at a very slow rate, with a period of order $100t_g$, from the ramps into the straight section (DTV in Fig. 3). In the interior of the straight section, one or two pairs of vortices disappear periodically. This is illustrated in Fig. 9, which is a contour plot for apparatus II of the straight section for $\Omega = 4.0$ and $R/R_c - 1 = 0.07$. Preliminary results show that the drift velocity has a maximum as R increases, and then decreases to zero. We consider it unlikely that the drift of the vortices is a feature of the axially uniform system under external rotation. Rather, we expect that the drift is induced by the selection of an unstable state by the ramps at the two ends of the system. Although it is known that the ramps used in our apparatus select a stable state in the *absence* of rotation,[22–24] the selection of unstable states has been predicted theoretically[28] and found experimentally[29] for the case where both the inner and the outer cylinder radii vary axially. We presume that the rotation has altered the wavenumber selection so dramatically that the selected wavenumber is unstable just above the onset of vortex flow. This interesting phenomenon is under further investigation.

As R is increased further in this range of Ω, a second transition occurs from tilted vortices to wavy tilted vortices (WTV in Fig. 3). This transition takes place at rather high R for our radius ratio. For the radius ratios used by Wiener *et al.*[15] the wavy mode at small Ω occurs at much smaller R. In our system this secondary bifurcation is hysteretic in the presence of rotation. We have not made a direct determination of the azimuthal mode

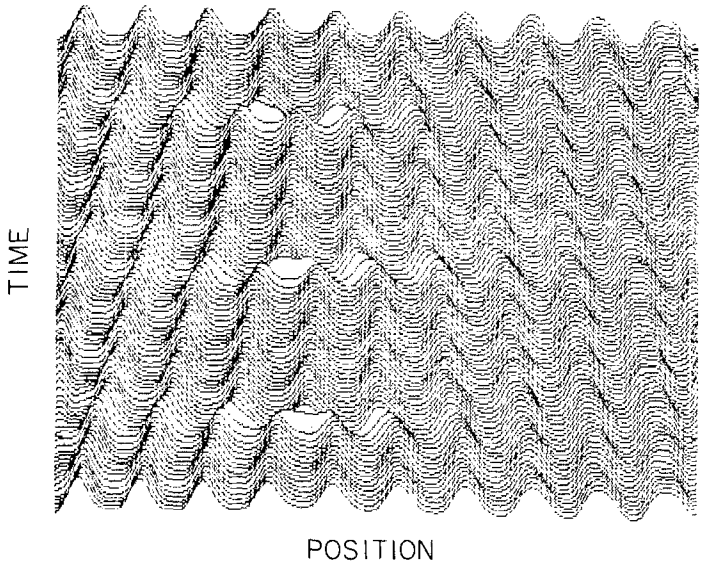

Fig. 9. Contour plot of the drifting tilted vortices in the center straight section of apparatus II for $\Omega = 4.0$ and $R/R_c - 1 = 0.07$. The time difference between successive contour lines is $1.4t_g$. The drifting waves of vortices entering the system from each end are apparent. They produce a periodic loss of vortex pairs in the interior of the straight section.

number m of this wavy mode. However, the ratio between the frequency ω_w of this mode and the frequency $\tilde{\omega}$ of the inner cylinder is about 0.8. Since the wavy-mode speed $(\omega_w/\tilde{\omega})/m$ is usually between 0.3 and 0.5,[30] we presume that m is at least 2 and probably not 3.

3.2. Medium Ω

At somewhat higher Ω (say from 5 to 15), the bifurcation sequence becomes more complicated. For $\Omega \lesssim 8.5$ a bifurcation from tilted vortices (DTV or STV) to a time-periodic tilted vortex state (PTV in Fig. 3) follows closely after the initial transition. This is shown in detail by the open diamonds in Figs. 3 and 4. This state differs from the wavy mode (WTV) at smaller Ω and large R which we discussed in the previous section, in that it has a relative frequency $\omega_s/\tilde{\omega}$ which is smaller by about a factor of two. Experimental results for $\omega_s/\tilde{\omega}$ are shown in Fig. 10 to the left of the vertical line at $\Omega = 8.5$. The open squares are for apparatus I, and the solid circle was obtained with apparatus II. The results agree well, and indicate that this mode is not significantly influenced by the nature of the cylinder ends.

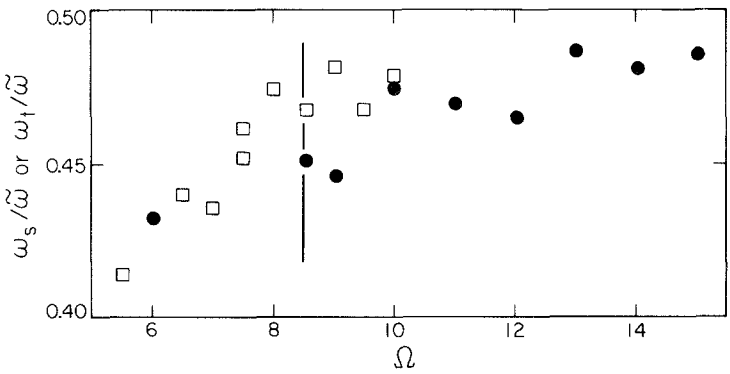

Fig. 10. The ratio of the periodic tilted-vortex (PTV) frequency ω_s or traveling tilted-vortex (TTV) frequency ω_t to the inner-cylinder frequency $\tilde{\omega}$ as a function of Ω. Open squares: Apparatus I (straight ends). Solid circles: Apparatus II (linear ramps). The data to the left of the vertical line at $\Omega = 8.5$ are for PTV which form at the secondary bifurcation. The data to the right of that line are for the primary bifurcation.

The secondary bifurcation to time-periodic tilted vortices becomes the first bifurcation at $\Omega \cong 8.5$. For somewhat larger Ω, the primary transition becomes one from structureless flow to *traveling* tilted vortices (TTV in Fig. 3). We emphasize that these time-periodic modes are unrelated to the drifting state (DTV) encountered at smaller Ω and discussed in the previous section. For the mode under discussion in the present section (TTV) the vortices are traveling in the same direction throughout the system, whereas the drifting waves at smaller Ω were moving in opposite directions at opposite ends of the apparatus (see Fig. 9). The frequencies ω_t of the traveling waves are two orders of magnitude larger than the frequencies of the drifting vortices at small Ω. The traveling-wave frequency ω_t evolves, within experimental resolution, continuously as a function of Ω from the frequency ω_s of the periodic tilted vortices. This is shown in Fig. 10. It is possible to prepare a state of traveling vortices which propagates in either direction, and we thus regard this bifurcation as a Hopf bifurcation. Since the frequency and bifurcation line of the PTV are continuous with those of the TTV, we presume that the secondary bifurcation to PTV is also a Hopf bifurcation. This implies that there is a complex conjugate *pair* of eigenvalues acquiring positive real parts at the secondary bifurcation to PTV, and that these eigenvalues evolve continuously into the pair associated with the primary bifurcation to TTV as Ω is increased. The relative stability of traveling vs. standing waves will be determined by nonlinear interactions and cannot be decided from linear stability analysis. We note that this situation is very different from that encountered in wavy

TVF. In that case the waves are azimuthal and only travel in the direction of the inner-cylinder rotation. They correspond to a *single* complex eigenvalue acquiring a positive real part, and thus we do not believe that the PTV discussed here are directly related to wavy vortex flow. This interesting bifurcation problem is under further investigation.

Upon increasing R further in this range of Ω (5 to 15), the pattern undergoes a transition to a chaotic state (CTV in Fig. 3). At even larger R, the flow returns through a hysteretic transition, shown in Figs. 3 and 4 as triangles, to a time-independent tilted vortex state. This hysteretic transition was investigated at fixed R by varying Ω. The chaotic vortices occur away from the ends and only exist in the central portion of apparatus II and III. This excludes the possibility that the transition is induced by the fixed boundaries. At the large-Ω end of this transition, the flow becomes generally turbulent even within the vortex structure itself, and we aborted the effort to locate the transition.

3.3. Large Ω

Upon increasing Ω to above 15, the state above the primary bifurcation becomes more and more irregular, and the bifurcation gradually becomes a direct transition to (visually) structureless turbulence (ST in Fig. 3). This turbulent state is different from those observed in Taylor–Couette flow without external rotation in that the latter still possess the Taylor-vortex structure, and the turbulence is on a smaller scale (see ref. 12 for a recent review). In the turbulent state observed here there is no large-scale structure, such as that of vortices, discernible. We observed that the transition from the laminar to the turbulent state becomes hysteretic for a range of Ω in the apparatus with either kind of ramp (apparatus II and III). We have not observed hysteresis in apparatus I. The hysteresis is illustrated in Fig. 5 for the case of apparatus II (linear ramps). The sizes and ranges of the hysteresis are qualitatively the same for the two different ramps, but depend quantitatively on the detailed shapes of the ramps. Although it is consistently found that the onset of the turbulence is triggered by the irregular flows which at these large values of Ω are generated at the fixed boundaries and which propagate into the bulk flow from the ends, in apparatus III (with doubly parabolic ramps) the flow near the ends of the apparatus is observed to be laminar when the bulk flow is turbulent after R is decreased from the onset of turbulence into the hysteretic region. Also the lower boundary of the hysteresis (in the Ω–R plane) smoothly joins the bifurcation line at higher and lower Ω within the experimental uncertainty. This evidence suggests that the turbulence is likely to be a bulk property of the flow.

At yet higher Ω ($\Omega \gtrsim 85$), the flow becomes rather complicated even in the base state. We aborted the effort to determine the bifurcation behavior for this portion of the parameter space.

Figure 11 shows a logarithmic plot of R_c vs. Ω for the lowest bifurcation as measured in each of the three apparatus. Within our possible systematic errors, $R_c(\Omega)$ is the same for the three outer cylinders used in our work. Contrary to the original expectations of Wiener *et al.*,[15] no asymptotic power-law behavior is evident at high Ω. If we nevertheless extract an ad hoc *effective* exponent from the data at large Ω (say $45 \lesssim \Omega \lesssim 200$), we obtain about 0.61. Previous work[15] had indicated that the data for $\Omega \lesssim 12$ were consistent with the value 4/3 obtained theoretically[4] for RBC with rotation. The more recent data of Wiener *et al.*[16] for Ω up to 22 and for $\eta = 0.883$ have also shown a slower increase of R_c with Ω than had originally[15] been expected. Thus, TVF with a Coriolis force differs from the prediction[4] for RBC with a Coriolis force. We do not know of any reason why the two systems should behave similarly. In the RBC case, the theoretical analysis[4] is based upon the assumption that a particular wavenumber first acquires a positive growth rate.[10] In the TVF case at large Ω we know from experiment that there is no well-defined

[10] One of us (G.A.) is grateful to H. R. Brand for discussions of this issue.

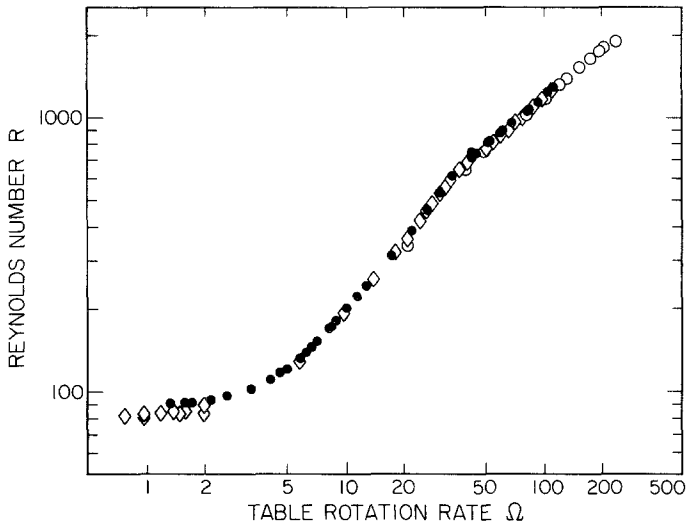

Fig. 11. Data for the primary bifurcation from all three apparatus on double logarithmic scales. Diamonds: Apparatus I. Solid circles: Apparatus II. Open circles: Apparatus III.

wavenumber, since the first state beyond the bifurcation is a featureless turbulent state. In addition, as mentioned above, the Coriolis force has a strong effect on the base state for TVF, but has no such effect in the RBC system. The data in Fig. 11 also indicate that there is at least one discontinuity in the slope of $R_c(\Omega)$, namely near $\Omega = 42$. It is beyond this value of Ω that the first bifurcation leads to the structureless turbulent state. Although not clearly resolved by our data, we expect that there is also a slope discontinuity near $\Omega = 8.5$ where the bifurcation line to STV or DTV meets the Hopf bifurcation line to PTV or TTV.

4. SUMMARY

We have presented quantitative experimental results for Taylor-vortex flow with rotation about an axis orthogonal to the cylinder axes. We made measurements in three apparatus which differed in the way in which the ends were terminated. In two of them, spatial ramps provided a gradual decrease in the axial direction of R below the critical value, and the other had an axially uniform geometry. Our apparatus had a radius ratio η close to 0.75. Our results are consistent with those of Wiener *et al.*[15,16] at larger values of η. In parallel to the experimental work, Ning *et al.* have calculated the linear properties at the primary bifurcation in this system as a function of the external rotation rate Ω.[20] The theoretical results agree very well with all available experimental data for $R_c(\Omega)$ at small values of Ω. A more detailed comparison between experiment and theory has been presented elsewhere.[21] The excellent agreement indicates a quantitative understanding of the primary bifurcation at small Ω, and opens the way for future detailed studies of a number of interesting phenomena which occur in this system. These phenomena include unexpected unstable wavenumber selection by spatial ramps which lead to drifting tilted vortices (DTV) near the onset of vortex flow, a secondary Hopf bifurcation to a time-periodic tilted vortex state (PTV), and a primary bifurcation to a traveling wave of tilted vortices (TTV). Particularly intriguing is the existence of a codimension-two point where the primary bifurcation to drifting or steady tilted vortices (DTV or STV) meets the Hopf bifurcation line to periodic or traveling (PTV or TTV) tilted vortices. At higher Ω, we have confirmed the existence of a turbulent state without any vortex structure (ST) which was discovered by Wiener *et al.*[16,17] We find that the transition to this state is hysteretic when the apparatus has spatial ramps at each end, and that for some parameter values the turbulence can be sustained even when the ramps provide a laminar region between the interior straight part of the system and the ends.

ACKNOWLEDGMENTS

We are grateful to R. J. Donnelly, P. W. Hammer, and R. J. Wiener for exchanging information on their parallel work prior to publication. We would also like to thank H. R. Brand and F. Busse for helpful discussions. This research was supported by the National Science Foundation under grant NSF-DMR88-14485.

REFERENCES

1. Lord Rayleigh, *Phil. Mag.* **32**:529 (1916).
2. H. Bénard, *Rev. Gen. Sci. Pure Appl.* **11**:1261, 1309 (1900); *Ann. Chim. Phys.* **23**:62 (1901).
3. E. L. Koschmieder, *Adv. Chem. Phys.* **26**:177 (1974); E. L. Koschmieder, *Order and Fluctuations in Equilibrium and Nonequilibrium Statistical Mechanics*, XVIIth International Solvay Conference, G. Nicolis, G. Dewel, and J. W. Turner, eds. (Wiley, New York, 1981), p. 168; F. Busse, in *Hydrodynamic Instabilities and the Transition to Turbulence*, H. L. Swinney and J. P. Gollub, eds. (Springer, Berlin, 1984), p. 97; F. Busse, *Rep. Prog. Phys.* **41**:1929 (1978).
4. S. Chandrasekhar, *Hydrodynamic and Hydromagnetic Stability* (Oxford University Press, London, 1961).
5. G. Küppers and D. Lortz, *J. Fluid Mech.* **35**:609 (1969).
6. R. M. Clever and F. H. Busse, *J. Fluid Mech.* **94**:609 (1979).
7. F. H. Busse and K. E. Heikes, *Science* **208**:173 (1980).
8. K. Bühler and H. Oertel, *J. Fluid Mech.* **114**:261 (1982).
9. P. G. J. Lucas, J. M. Pfotenhauer, and R. J. Donnelly, *J. Fluid Mech.* **129**:251 (1983).
10. J. M. Pfotenhauer, J. J. Niemela, and R. J. Donnelly, *J. Fluid Mech.* **175**:85 (1987).
11. G. I. Taylor, *Phil. Trans. R. Soc. Lond. A* **223**:289 (1923).
12. R. C. DiPrima and H. L. Swinney, in *Hydrodynamic Instabilities and Transitions to Turbulence*, H. L. Swinney and J. P. Gollub, eds. (Springer, Berlin, 1981).
13. D. Coles, *J. Fluid Mech.* **21**:385 (1965); H. A. Snyder, *J. Fluid Mech.* **35**:273 (1969); J. E. Burkhalter and E. L. Koschmieder, *Phys. Fluids* **17**:1929 (1974).
14. A. Mallock, *Proc. R. Soc.* **1888**(13 December), 126; *Phil. Trans. R. Soc. Lond. A* **187**:41 (1895); M. M. Couette, *Compt. Rend.* **107**:388 (1888); *Ann. Chem. Phys. VI* **21**:433 (1890).
15. R. J. Wiener, P. W. Hammer, C. E. Swanson, and R. J. Donnelly, *Phys. Rev. Lett.* **64**:1115 (1990).
16. R. J. Wiener, P. W. Hammer, C. E. Swanson, D. C. Samuels, and R. J. Donnelly, *J. Stat. Phys.*, this issue.
17. R. J. Wiener, P. W. Hammer, C. E. Swanson, and R. J. Donnelly, private communication.
18. H. R. Brand, private communication.
19. R. J. Wiener, private communication.
20. L. Ning, M. Tveitereid, G. Ahlers, and D. S. Cannell, *Phys. Rev. A.*, in press.
21. L. Ning, G. Ahlers, D. S. Cannell, and M. Tveitereid, *Phys. Rev. Lett.* **66**, 1575 (1991).
22. D. S. Cannell, M. A. Dominguez-Lerma, and G. Ahlers, *Phys. Rev. Lett.* **50**:1365 (1983).
23. M. A. Dominguez-Lerma, D. S. Cannell, and G. Ahlers, *Phys. Rev. A* **34**:4956 (1986).
24. G. Ahlers, D. S. Cannell, M. A. Dominguez-Lerma, and R. Heinrichs, *Physica* **23D**:202 (1986).
25. P. Matisse and M. Gorman, *Phys. Fluids* **27**:759 (1984).

26. M. A. Dominguez-Lerma, Ph.D. Thesis, University of California at Santa Barbara (1986).
27. M. A. Dominguez-Lerma, G. Ahlers, and D. S. Cannell, *Phys. Fluids* **27**:856 (1984).
28. H. Riecke and H. G. Paap, *Phys. Rev. Lett.* **59**:2570 (1987).
29. L. Ning, G. Ahlers, and D. S. Cannell, *Phys. Rev. Lett.* **64**:1235 (1990).
30. G. Ahlers, D. S. Cannell, and M. A. Dominguez-Lerma, *Phys. Rev. A* **27**:1225 (1983).